Filamenting-ring-Airy-beam femtosecond pulse in air at 10 m through quasi-Gaussian beam modulation with a dedicated phase plate

Yunfei Rao,[1] Tianyang Sun,[1] Chen Sun,[1] Long Zou,[1,2] Arnaud Couairon,[2,*] and Jin Yu[1,†]
[1]School of Physics and Astronomy, Shanghai Jiao Tong University, Shanghai 200240, China
[2]CPHT, CNRS, Ecole Polytechnique, Institut Polytechnique de Paris, F-91128 Palaiseau, France

(Received 1 June 2024; accepted 2 August 2024; published 23 August 2024)

Femtosecond laser filamentation in air presents significant potential for atmospheric scale applications, including remote sensing and lightning control. However, projecting a filament over large distances remains a challenge due to the complex nonlinear propagation dynamics of high-intensity femtosecond pulses. This work demonstrates the generation of an intense ring-Airy-beam femtosecond pulse in air, employing a specially designed phase plate that converts an input quasi-Gaussian beam into the Fourier transform of a ring Airy beam at the front focal plane of a Fourier lens. The high damage threshold of the phase plate enables the corresponding near field of the ring Airy beam at the rear focal plane of the lens to reach a tens-of-gigawatt peak power. This near field subsequently evolves, at a distance of 10 m, into an ionizing filament, capable of ablating an aluminum plate and performing laser-induced breakdown spectroscopy (LIBS). Extending the cm-scale propagation of a ring Airy beam in liquids or glasses, as reported in previous works, to the 10-meter scale with the generation of an ionizing filament, represents a crucial step toward real-world applications of remote LIBS with ring-Airy-beam femtosecond pulses. Experimental observations show a filament length of two meters, corroborating the numerical simulation and expanding the potential to applications that necessitate a long plasma channel. Further numerical simulations indicate the feasibility of controlling the starting point of a filament beyond 100 meters by increasing the focal length of the Fourier lens, opening avenues for fascinating applications in remote sensing and beyond.

DOI: 10.1103/PhysRevA.110.023521

I. INTRODUCTION

Femtosecond laser filaments, owing to their high peak power and distinctive propagation properties, have found significant applications in atmospheric sciences [1,2], particularly in remote sensing [3–7] and lightning control [8]. However, the task of efficiently projecting femtosecond filament to a predetermined location over extended atmospheric distances, together with the precise control of filament parameters such as initiation point, filament length, optical intensity, and electron density within the associated plasma channels, is highly challenging and critically important [9,10].

For Gaussian beam femtosecond pulses, techniques such as group velocity dispersion precompensation and telescope-based beam collimation have been proposed and implemented [2,11], enabling an increase in the filamentation starting distance. However, focusing femtosecond pulses through telescopic systems with prechirp leads to a gradual increase in peak intensity, resulting in a low contrast in intensity, rendering the system susceptible to multiple filament generation [12,13]. The instability in multiple filamentation, characterized by significant variability in the spatial positions and transverse dimensions of filaments and plasma channels along their propagation paths, presents major challenges in predicting filamentation distances and accurately positioning filaments at a predetermined location. Additionally, the long-range projection of femtosecond laser filament inherently encounters nonlinear losses, such as those arising from air ionization during plasma channel formation [14].

Ring Airy beams, introduced as cylindrically symmetric Airy beam profiles [15,16], inherit the transverse acceleration of their intensity peak from Airy beams [17,18], a feature that is also clearly evident in the filamentation characteristics of Airy beams [19,20]. Ring Airy beams possess the unique ability to autofocus along a parabolic trajectory, culminating in a significant amplification of its peak intensity at the focal point [15,16]. Owing to these properties, ring Airy beams demonstrate substantial promise for diverse applications across several fields, including microparticle trapping and guiding [21,22], biomedical cell manipulation [23], femtosecond laser filamentation [24–26], harmonic generation [27], multiscale photopolymerization [28], as well as the generation of air plasma and terahertz wave [29]. In these applications without need of a large operation distance, ring Airy beams with relatively short autofocusing distances have typically been sufficient. In addition, high peak intensity in the focal region is also not always required, which leads to the common use of a spatial light modulator (SLM) for the generation of ring Airy beams.

On the other hand, due to its self-accelerating property, a ring Airy beam has the ability to achieve a unique abrupt autofocus with high contrast without the need of an

*Contact author: arnaud.couairon@polytechnique.edu
†Contact author: jin.yu@sjtu.edu.cn

additional lens at a remote distance. Unlike the Airy beam, where increasing the power results in a filament with a parabolic high-intensity trajectory [19,20], the power of a ring Airy beam can be increased while maintaining a linear autofocusing stage followed by a distinct filamentation stage beyond the focus. This characteristic allows for avoiding nonlinear losses [15,16] and the projection of a single filament over long distances. To evaluate the feasibility of employing a ring Airy beam for remote filamentation, recent numerical simulations present a scenario of projecting a high power density at kilometric distances [10], showing the capability of ring Airy beams to achieve precisely remote laser energy deposition. This reference, however, did not provide comprehensive experimental validation or thoroughly explore specific experimental methods for generating ring Airy beams with large autofocusing distances. Additionally, there is little discussion of the detailed filamentation process and related applications, such as filament-induced breakdown spectroscopy.

New applications of ring Airy beams thus emerge on a significantly broader spatial scale, involving the propagation of femtosecond laser filaments through the atmosphere. Such applications require the autofocusing distance of a ring Airy beam to span from tens to hundreds of meters. Additionally, the peak intensity at the focus region is required to surpass the air ionization threshold to initiate and maintain a strong and stable filament. Facing these applications, the conventional generation method with wavefront modulation using a SLM meets substantial limitations, stemming from its low damage threshold and restricted modulation region and low spatial resolution of the phase distribution.

In this work, we demonstrate the generation of a ring-Airy-beam femtosecond pulse at a peak power level of tens of gigawatts by modulating an initial Gaussian beam femtosecond laser pulse with a specially designed phase plate. Our experimental results, supported by a dedicated numerical simulation, show the evolution of the ring-Airy-beam pulse into an ionizing filament at a distance of about 10 m and over a distance of about 2 m, indicating a significant meter-long region of high intensity and plasma generation beyond the autofocusing distance. The generated filament is able to ablate an aluminum target, allowing us to perform laser-induced breakdown spectroscopy (LIBS) on the target. A customized phase plate with an imprinted phase-modulation pattern was employed in a Fourier-transform-based setup as an effective alternative to an SLM with a much higher damage threshold, which exceeds that of an SLM by orders of magnitude. The comprehensive numerical simulation offers additional insights into the filament's properties, which are challenging to ascertain with our experimental setup. This includes distributions of light intensity and plasma density at high spatial resolution within the filament, thus enriching the characterization of the generated filament for a broader range of applications. Further theoretical analysis indicates the potential to control the starting point of the filamentation to a longer distance of 100 m by combining the actual phase plate with a Fourier lens of longer focal distance. Consequently, this study represents a significant milestone in extending the application of ring Airy beams to much greater atmospheric distances.

II. METHODS

A. Experimental implementation

In the experiment, the Fourier transform method was employed to generate a ring Airy beam [16]. The corresponding experimental setup is shown in Fig. 1. In brief, Fourier transform is applied to the near field of a given ring Airy beam to be generated. The phase distribution function obtained is then imprinted onto a glass plate. The resulting phase plate is inserted into the propagation path of a quasi-Gaussian beam and located on the front focal plane of a Fourier lens, as shown in Fig. 1(a). The phase-modulated wave front of the beam is subsequently inversely Fourier transformed by the lens, resulting in the near field of the desired ring Airy beam on the rear focal plane of the Fourier lens. Since the Fourier transform of the near field of a ring Airy beam lacks analytical form, an approximative expression is used [30],

$$U(k) = \left(\frac{r_0}{w_0} + k^2 w_0^2\right) \exp\left(-\alpha k^2 w_0^2\right) \times \sqrt{\frac{3kr_0 + k^3 w_0^3}{3kr_0 + 3k^3 w_0^3}} J_0\left(kr_0 + \frac{k^3 w_0^3}{3}\right), \quad (1)$$

where r_0 represents the radius of the primary ring of the near field intensity distribution, α is a dimensionless truncation constant, w_0 is a scaling factor, $k = 2\pi r/\lambda f$ is the radial spatial frequency, r is the radial coordinate, $\lambda = 800$ nm is the central wavelength of the femtosecond laser pulses, and $f = 2000$ mm is the focal length of the Fourier lens. In the experiment, w_0, r_0, and α were, respectively, set to 0.4 mm, 6.0 mm, and 0.05. For the resulting near field, the theoretical linear autofocusing distance can be calculated as $f_{Ai} = 4\pi w_0^2 \sqrt{r_0/w_0 + 1}/\lambda$. In the experiment, this distance was fixed at 10.05 m to facilitate an implementation in our laboratory. Figure 1(b) presents the calculated phase pattern according to Eq. (1), and Fig. 1(c) focuses on the central region demarcated by a red dashed square in Fig. 1(b), highlighting the zone of the most significant phase modulation. Figure 1(d) depicts the relative phase profile of the phase pattern taken along the radial direction from its center. The calculated phase pattern was imprinted on a 25.4-mm-diameter glass substrate by Lubon Technology Co., Ltd., using the liquid crystal beam splitter technology [31,32].

A chirped pulse amplification (CPA) Ti:sapphire femtosecond laser (ARCO H, Amplitude Laser, Inc.) emitted 10 Hz, 30 mJ, 35 fs laser pulses around a wavelength of 800 nm, with a near top-hat intensity distribution of 3-cm diameter and a Gaussian temporal distribution (Fig. 1). A beam-reducing arrangement, comprised of a plano-convex lens ($f = 300$ mm) and a plano-concave lens ($f = -150$ mm), was utilized to condense the laser beam section to half of its original diameter. At the same time, we ensured that the reduced beam did not present any visible nonlinear optical effect while transmitting the involved lenses and the phase plate. Such a beam concentration increased the power density, allowing a maximum energy carried by a pulse being effectively modulated. After passing through the beam-reducing arrangement, the pulse propagated toward the phase plate located on the front focal plane of a convergent lens of 2-m focal length serving as the Fourier lens, where the wave front of the pulse was

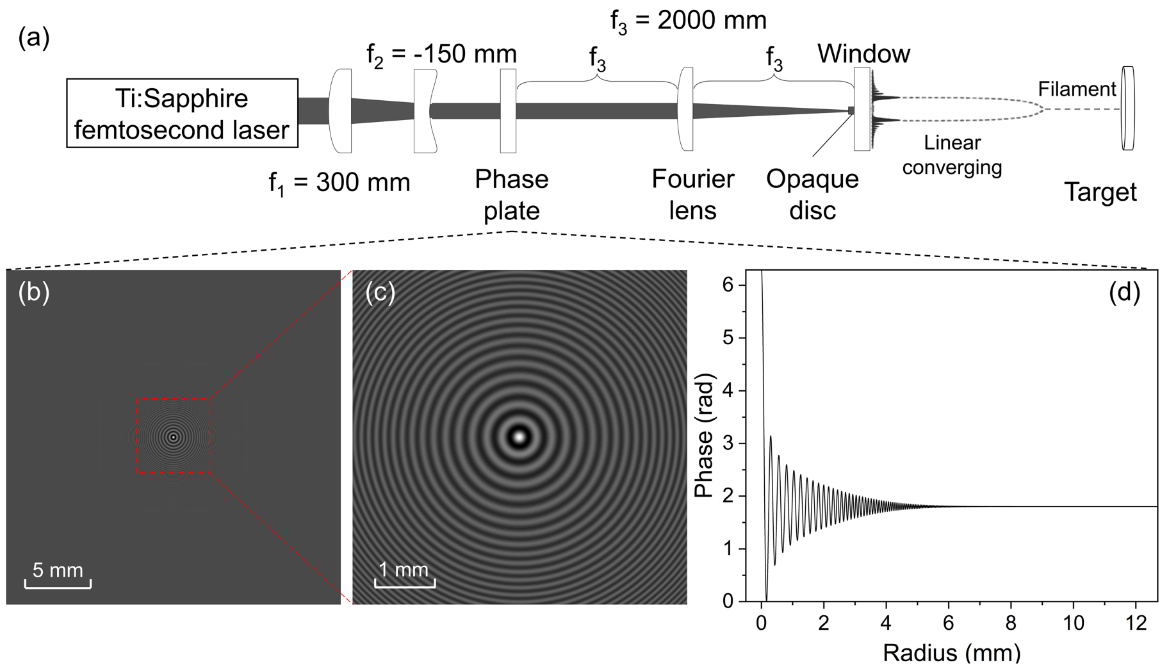

FIG. 1. Experimental setup for ring Airy beam generation with, in particular, the calculated phase pattern. (a) Schematic of the experimental setup. (b) Computed phase distribution. (c) Enlarged view of the central region delimited by the red dashed square in (b). (d) Relative phase as a function of the radial distance from the center of the phase plate.

modulated by the imprinted phase function. The modulated pulse then propagated through the Fourier lens. The Fourier transform of the near field of a ring Airy beam on the front focal plane of the lens was inversely transformed back to its near field distribution on the rear focal plane. In reality, the diffraction through the Fourier lens presented a zero-order pattern at the center of the distribution on the rear focal plane of the lens. Theoretically, in order to generate ring Airy beams, both amplitude and phase modulation are required. However, in the experiment, only phase modulation was used without the application of amplitude modulation. Consequently, parts of laser intensities that would normally be attenuated by an amplitude modulation remained unchanged. This portion of the laser beam is then focused by the Fourier lens, forming a light spot at the focal point. Moreover, as shown in Fig. 1(d), for the area of the phase plate with a radius exceeding 6 mm, there is almost no phase-modulation effect on the incident laser beam, resulting in practically unmodulated intensities. This unmodulated portion of the beam will also be focused by the Fourier lens, generating the central spot at the focal plane. Therefore, this central spot did not contribute to the near field of the ring Airy beam. It is why a metallic disk of 5-mm diameter was installed at the axis on the rear focal plane of the lens in order to block the zero-order pattern of the distribution. A measurement with an energy meter (Gentec-EO) resulted in a reduced pulse energy of 2.24 mJ and a corresponding peak power of about 64 GW. Such a reduction accounted for the above-mentioned loss in the zero order of diffraction and the losses due to the reflections on the optical interfaces of the involved optical elements. The above generated near field of the ring Airy beam pulse propagated in the laboratory and was characterized during its evolution into a filament at a distance of about 10 m. The limited space in the laboratory imposed upon us the use of four high-reflection flat mirrors to fold up the optical path. This led to an attenuation of the pulse due to the reflections on the mirrors, but also the truncation of the beam on the mirrors, resulting in a transmitted pulse energy of 1.71 mJ, which corresponded to a peak power of 48.9 GW for a pulse duration of 35 fs. This energy level resulted in the formation of a single filament in the experiment.

The linear converging of the beam was monitored by inserting a graph paper featuring a fine square grid, at different distances between the rear focal plane of the Fourier lens, considered as the origin of the propagation, and the inception of the filament. The images of intercepted beam sections were then photographed using a CCD camera in a nonsynchronized accumulation mode. The exposure time of the camera was adjusted to avoid its saturation. The inception and termination of the ionizing filament were ascertained using a polyvinyl-chloride (PVC) target, since its optical damage threshold intensity [33] is approximately $1 \times 10^{17}\ \mathrm{W/m^2}$, which is greater than the minimum intensity required for a detectable air ionization [34] of $8 \times 10^{16}\ \mathrm{W/m^2}$. By displacing the PVC target in the beam and looking at the appearance and disappearance of surface damage on it, we determined the position and extension of the air plasma channel generated by the ring-Airy-beam filament. For the recording of the surface damage patterns on the PVC target, we accumulated 600 laser shots over a period of 60 seconds.

The ionizing filament was finally intercepted by an aluminum plate at normal incidence. A spark of white light was observed on the surface of the plate, attesting to the generation of a laser-induced plasma. The plasma emission was collimated along an axis making an angle of about 45° with respect to the filament, by an optical arrangement consisting of a pair of quartz lenses of focal length of 100 mm. An optical fiber of

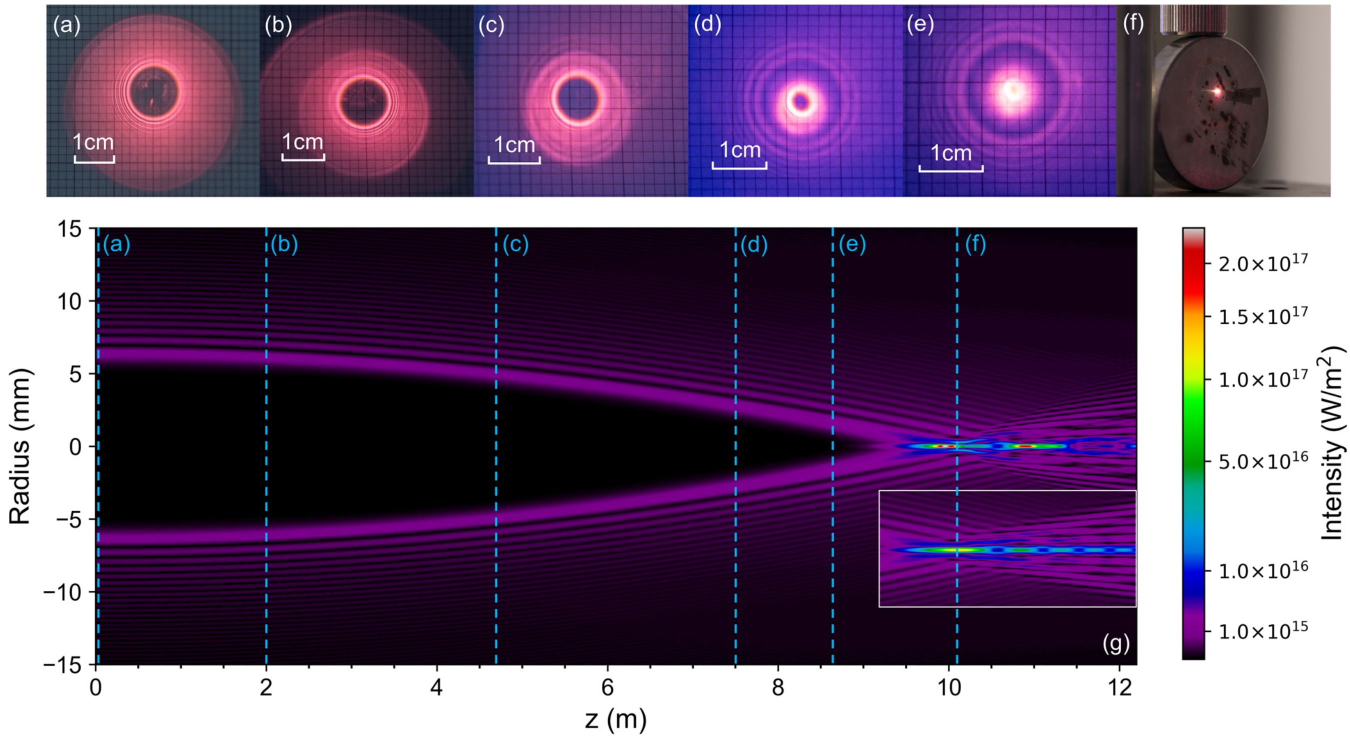

FIG. 2. Experimental intensity profiles of a ring-Airy-beam pulse and the corresponding numerical simulation, together with a comparison in the beam focusing region, with the linear propagation: (a) at the rear focal plane of the Fourier lens considered as the origin of the propagation distance, z, (b) at 200 cm, (c) at 470 cm, (d) at 750 cm, and (e) at 865 cm with respect to the origin. (f) A picture of an aluminum target at 10.08 m with a filament-induced spark characterized by intense white and reddish hues, indicative of its high temperature. (g) Simulation result with the near field of the experimental ring Airy beam as the initial condition. Inset: The beam profile beyond 9 m and presented in the same scales of the corresponding linear propagation when the nonlinear terms are set to zero in the propagation equation.

50-µm core diameter was placed at the focal point of the collection arrangement and captured a part of the collected light. The fiber was connected to an echelle spectrometer (Mechelle 5000, Andor Technology) equipped with an intensified charge coupled device (ICCD) camera (iStar, Andor Technology), to record the spectrum of the collected plasma emission. The Q-switch signal from the pump laser of the CPA amplifier was used to synchronize the ICCD camera set with a detection delay and gate width of, respectively, 150 ns and 10 µs.

B. Numerical simulation

The propagation of the ring-Airy-beam pulse was numerically simulated to describe in detail the evolution of the pulse from its near field on the rear focal plane of the Fourier lens to the filament. The simulation result was compared to the experimental observations, which validated the theoretical model. The validated theoretical model further offers a more comprehensive and in-depth analysis of the propagation process. A well-established numerical model, known as the nonlinear envelope model [14], was employed to simulate the propagation by taking into account both the linear and nonlinear propagation effects, including the diffraction, the optical Kerr effect, the multiphoton absorption (MPA), and the plasma defocusing. The principle and detailed implementation of the numerical simulation have been thoroughly presented in our previous works [10,35]. In this work, the experimentally generated near field was used as the initial condition, permitting an end-to-end simulation of the real experiment. Experimental fluctuations were taken into account in the simulation, including 10% of pulse energy fluctuation around 1.71 mJ, 10% of amplitude fluctuation with respect to the interval between the maximal and the minimal amplitude values, and a white noise on the phase within the interval of $[-\pi/10, \pi/10]$.

III. RESULTS AND DISCUSSION

Figures 2(a)–2(e) present a series of five CCD images showing the intensity profile of a ring Airy beam acquired in the experiment at increasing distances from the rear focal plane of the Fourier lens. From one image to the next, the central dark region of the beam diminishes in size, leading to a concentration of the pulse energy along the propagation axis. Figure 2(f) captures emissions from the plasmas induced by filamenting-ring-Airy-beam pulses on the aluminum target placed at a distance of 10.08 meters from the rear focal plane of the Fourier lens. The corresponding simulation results are shown in Fig. 2(g), depicting the intensity profile of a ring-Airy-beam pulse as a function of the propagation distance z, resulting from a single typical simulation. We can see that the initial propagation stage is predominately linear with an intensity smaller than 1×10^{16} W/m^2, where the ring Airy beam undergoes a linear self-converging. At a distance of about 9.5 m, the axial intensity increases beyond 5×10^{16} W/m^2

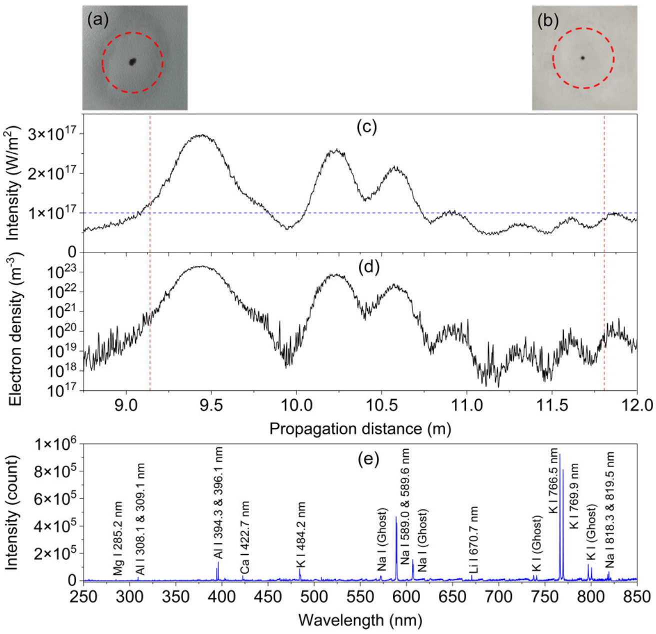

FIG. 3. Experimental beam impacts on a PVC target inserted in the beam at (a) 9.14 m and (b) 11.80 m, highlighted by dashed red circles. Numerical simulations of (c) the intensity and (d) the electron number density in the filamentation region. (e) Typical emission spectrum of the plasmas induced by a ring-Airy-beam filament on the aluminum target. The main emission lines are indicated according to the NIST atomic spectra database [36].

and obvious nonlinear self-focusing occurs, leading to the appearance of a filament showing a multiple intensity maxima with a maximal intensity exceeding 2×10^{17} W/m^2. The intensity in the filament is sufficiently high to initiate an air ionization, leading to the creation of significantly dense air plasma along the propagation axis. At a distance of about 10.5 m, we can observe a damping of the first segment of filament. A second segment of filament appears due to the self-focusing of the diffracted optical pulse, leading to multiple maxima with a maximal intensity exceeding 1.5×10^{17} W/m^2. The ensemble of the two segments of filament sustains a high-intensity propagation zone extending 2 meters, indicating the formation of a strong, quasicontinuous filament with a significant ionization of air. A linear propagation of the same input ring-Airy-beam pulse has been simulated using the same numerical simulation program by setting the nonlinear terms to zero in the propagation equation, including the Kerr self-focusing and the multiphoton absorption terms. The obtained result is shown in the inset of Fig. 2(g) in the focus region and with the same space and intensity scales. We can see that the linear propagation leads to a primary focus and several secondary foci with intensities of the order of 1×10^{17} W/m^2, which would induce a weak ionization of the air over a limited space extension. In addition, the secondary foci are much weaker than the primary one in the absence of nonlinear self-focusing.

In order to precisely determine the extension of the filament, we exposed a PVC target to the beam at different propagation distances, and found that beyond a distance of 914 cm from the rear focal plane of the Fourier lens, the target became clearly marked when exposed to the beam for one minute, as shown in Fig. 3(a).

We found that the impact remained visible up to a distance 1180 cm for an exposure of one minute, as shown in Fig. 3(b). The above two positions can therefore delimit the spatial extension of the filament. The experimental observation is numerically simulated by taking into account the experimental fluctuations, as explained above. Thus, a series of 600 simulations has been performed with randomly fluctuating experimental conditions. The result is presented with the average of the 60 simulations providing the highest maximal intensities and, correspondingly, the highest maximal electron number densities, as shown in Figs. 3(c) and 3(d). We can see that the detailed profile of the intensity in Fig. 3(c) shows three successive high-intensity zones delimiting a filament extension from 9.07 m to 11.87 m if we take an intensity of 1×10^{17} W/m^2 as the criterion of the filament, which is consistent with the experimental observations. Moreover, the numerical simulation provides a detailed profile of the electron number density within the filament, as shown in Fig. 3(d). Such information is not accessible with the used experimental setup. A typical emission spectrum of the plasmas induced on the aluminum target by the filament is finally shown in Fig. 3(e). We can see that the spectrum displays a series of well-defined emission lines corresponding to various elements contained in the target or deposited on its surface as contaminations with a high signal-to-noise ratio. Such a result demonstrates the perspective of LIBS application of the studied high-intensity ring-Airy-beam femtosecond pulses.

According to Eq. (1), the focal length of the Fourier lens f influences the phase pattern for a given linear self-focusing distance of the ring Airy beam f_{Ai}. This means that changing f modifies the phase pattern for a given f_{Ai}, while for a fixed phase pattern, f_{Ai} can be controlled by changing f. Such flexibilities are interesting, on the one hand, to better fit the effective modulation zone of the phase plate to the section of the input beam in order to increase the energy conversion efficiency to the ring Airy beam, and, on the other hand, to vary the linear self-focusing distance f_{Ai} of the ring Airy beam produced using a fixed phase plate. Such a combination effect is illustrated in Fig. 4 with calculated phase patterns and the associated relative phase functions. We can see in Figs. 4(a)–4(c) that for a given $f_{Ai} = 10$ m, an increasing focal length of the Fourier lens (2, 5, and 10 m) allows an enlargement of the effective phase-modulation zone. This should allow a better energy conversion efficiency from an incident quasi-Gaussian beam to a ring Airy beam by increasing the focal length of the Fourier lens. The same study is performed for a longer linear self-focusing distance of $f_{Ai} = 100$ m, as shown in Figs. 4(d)–4(f). We can see that with the Fourier lens of 2-m focal length used in this experiment, the generation of a ring Airy beam is practically impossible because of the smallness of the effective modulation zone on the phase plate and the high space frequency of the phase-modulation function. If a Fourier lens of 10-m focal length is employed, the required phase pattern for $f_{Ai} = 100$ m becomes quite similar to that for $f_{Ai} = 10$ m when combined with a Fourier lens of 2-m focal length, as shown in Fig. 4(f). These results thus demonstrate the potential to push a ring-Airy-beam filament

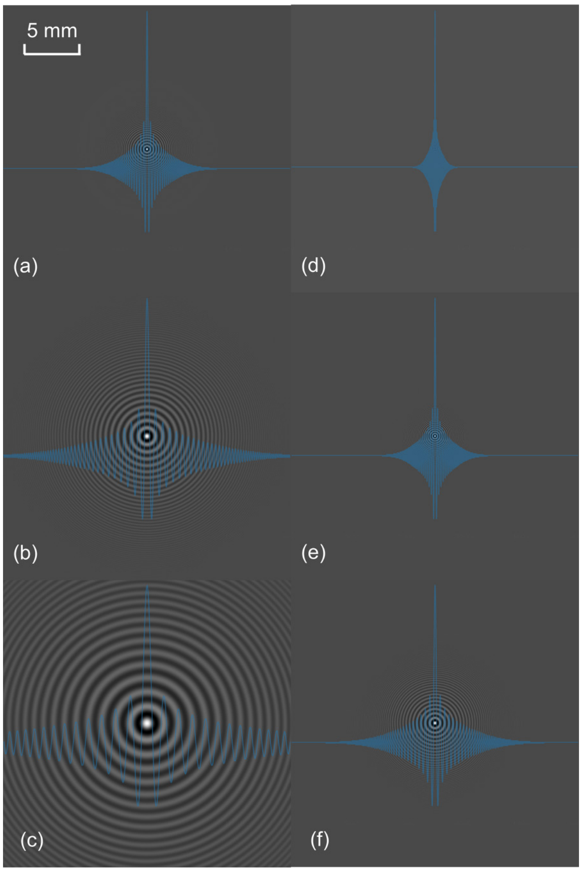

FIG. 4. Calculated phase distribution patterns and the associated relative phase functions presented on the same scale as that which should be imprinted on a glass plate to produce a linear self-focusing at (a)–(c) 10 m and at (d)–(f) 100 m, when associated with a Fourier lens of focal length of (a),(d) 2 m, (b),(e) 5 m, and (c),(f) 10 m.

to much larger distances with a flexible control by optimizing the combination between the phase plate and the Fourier lens.

IV. CONCLUSION

In conclusion, we have generated a ring-Airy-beam femtosecond pulse by using a dedicated phase plate in the configuration of the Fourier transform method for ring-Airy-beam production. The much higher damage threshold of the used phase plate than the usually used SLM allowed the near field of a ring Airy beam to be obtained with a pulse energy of 2.24 mJ, corresponding to a peak power of 64 GW within a pulse duration of 35 fs. The combination of the phase plate and a Fourier lens of 2-m focal length led the ring-Airy-beam pulse to self-focus at a distance of about 10 m, with the initiation of a filament of about 2.66 m length, and able to perform LIBS on a metal plate. An end-to-end numerical simulation showed a maximal intensity of about 3×10^{17} W/m^2 and an electron number density of the order of 10^{23} m^{-3} within the filament. A satisfactory LIBS spectrum was recorded with the plasmas induced by the filaments on an aluminum target placed at 10.08 m from the rear focal plane of the Fourier lens. Finally, an extension of the study with the numerical simulation shows the possibility to control the linear self-focusing distance of a ring Airy beam by an optimized combination between the phase plate and the Fourier lens, with a potential to generate a filament at a much larger distance of 100 m for atmospheric scale applications [1,7,8,37].

ACKNOWLEDGMENT

Y.R. acknowledges the support of the China Scholarship Council (202306230221).

[1] J. Kasparian, M. Rodríguez, G. Méjean, J. Yu, E. Salmon, H. Wille, R. Bourayou, S. Frey, Y.-B. André, and A. Mysyrowicz, Science **301**, 61 (2003).
[2] M. Rodriguez, R. Bourayou, G. Méjean, J. Kasparian, J. Yu, E. Salmon, A. Scholz, B. Stecklum, J. Eislöffel, U. Laux, A. P. Hatzes, R. Sauerbrey, L. Woste, and J. P. Wolf, Phys. Rev. E **69**, 036607 (2004).
[3] H. L. Xu and S. L. Chin, Sensors **11**, 32 (2010).
[4] H. Xu, Y. Cheng, S. Chin, and H. Sun, Laser Photon. Rev. **9**, 275 (2015).
[5] S. Chin, H. Xu, Q. Luo, F. Théberge, W. Liu, J. Daigle, Y. Kamali, P. Simard, J. Bernhardt, and S. Hosseini, Appl. Phys. B **95**, 1 (2009).
[6] J.-F. Gravel, Q. Luo, D. Boudreau, X. Tang, and S. Chin, Anal. Chem. **76**, 4799 (2004).
[7] I. Dicaire, V. Jukna, C. Praz, C. Milián, L. Summerer, and A. Couairon, Laser Photon. Rev. **10**, 481 (2016).
[8] A. Houard, P. Walch, T. Produit, V. Moreno, B. Mahieu, A. Sunjerga, C. Herkommer, A. Mostajabi, U. Andral, Y.-B. André *et al.*, Nat. Photon. **17**, 231 (2023).
[9] L. Zou, C. Sun, Y. Rao, T. Sun, J. Yu, and A. Couairon, Phys. Rev. Res. **4**, 043025 (2022).
[10] L. Zou, C. Sun, J. Yu, and A. Couairon, Phys. Rev. A **108**, 023524 (2023).
[11] G. Méchain, G. Méjean, R. Ackermann, P. Rohwetter, Y.-B. André, J. Kasparian, B. Prade, K. Stelmaszczyk, J. Yu, and E. Salmon, Appl. Phys. B **80**, 785 (2005).
[12] N. K. Efremidis, Z. Chen, M. Segev, and D. N. Christodoulides, Optica **6**, 686 (2019).
[13] D. Apeksimov, Y. E. Geints, A. Zemlyanov, A. Kabanov, V. Oshlakov, A. Petrov, and G. Matvienko, Appl. Opt. **57**, 9760 (2018).
[14] A. Couairon and A. Mysyrowicz, Phys. Rep. **441**, 47 (2007).
[15] N. K. Efremidis and D. N. Christodoulides, Opt. Lett. **35**, 4045 (2010).
[16] D. G. Papazoglou, N. K. Efremidis, D. N. Christodoulides, and S. Tzortzakis, Opt. Lett. **36**, 1842 (2011).
[17] G. A. Siviloglou and D. N. Christodoulides, Opt. Lett. **32**, 979 (2007).
[18] G. A. Siviloglou, J. Broky, A. Dogariu, and D. N. Christodoulides, Phys. Rev. Lett. **99**, 213901 (2007).
[19] P. Polynkin, M. Kolesik, and J. Moloney, Phys. Rev. Lett. **103**, 123902 (2009).

[20] M. Clerici, Y. Hu, P. Lassonde, C. Milián, A. Couairon, D. N. Christodoulides, Z. Chen, L. Razzari, F. Vidal, F. Légaré *et al.*, Sci. Adv. **1**, e1400111 (2015).
[21] P. Zhang, J. Prakash, Z. Zhang, M. S. Mills, N. K. Efremidis, D. N. Christodoulides, and Z. Chen, Opt. Lett. **36**, 2883 (2011).
[22] W. Lu, X. Sun, H. Chen, S. Liu, and Z. Lin, Phys. Rev. A **99**, 013817 (2019).
[23] Y. Liang, G. Liang, Y. Xiang, J. Lamstein, R. Gautam, A. Bezryadina, and Z. Chen, Phys. Rev. Appl. **12**, 064060 (2019).
[24] P. Panagiotopoulos, D. Papazoglou, A. Couairon, and S. Tzortzakis, Nat. Commun. **4**, 2622 (2013).
[25] P. Panagiotopoulos, A. Couairon, M. Kolesik, D. G. Papazoglou, J. V. Moloney, and S. Tzortzakis, Phys. Rev. A **93**, 033808 (2016).
[26] H. Yuze, N. Jinsong, S. Ke, and W. Lei, Infrared Laser Eng. **46**, 806005 (2017).
[27] A. D. Koulouklidis, D. G. Papazoglou, V. Y. Fedorov, and S. Tzortzakis, Phys. Rev. Lett. **119**, 223901 (2017).
[28] M. Manousidaki, D. G. Papazoglou, M. Farsari, and S. Tzortzakis, Optica **3**, 525 (2016).
[29] K. Liu, A. D. Koulouklidis, D. G. Papazoglou, S. Tzortzakis, and X.-C. Zhang, Optica **3**, 605 (2016).
[30] I. Chremmos, P. Zhang, J. Prakash, N. K. Efremidis, D. N. Christodoulides, and Z. Chen, Opt. Lett. **36**, 3675 (2011).
[31] D. Mawet, E. Serabyn, K. Liewer, C. Hanot, S. McEldowney, D. Shemo, and N. O'Brien, Opt. Express **17**, 1902 (2009).
[32] Z. Tong, Y. Yan, Y. Ma, M. Wang, S. Jia, and X. Chen, Opt. Lett. **46**, 3965 (2021).
[33] S. Eisenmann, E. Louzon, Y. Katzir, T. Palchan, A. Zigler, Y. Sivan, and G. Fibich, Opt. Express **15**, 2779 (2007).
[34] J. Kasparian, R. Sauerbrey, and S. Chin, Appl. Phys. B **71**, 877 (2000).
[35] A. Couairon, E. Brambilla, T. Corti, D. Majus, O. de J. Ramírez-Góngora, and M. Kolesik, Eur. Phys. J.: Spec. Top. **199**, 5 (2011).
[36] https://physics.nist.gov/PhysRefData/ASD/lines_form.html
[37] J. Kasparian, R. Ackermann, Y.-B. André, G. Méchain, G. Méjean, B. Prade, P. Rohwetter, E. Salmon, K. Stelmaszczyk, J. Yu, A. Mysyrowicz, R. Sauerbrey, L. Wöste, and J.-P. Wolf, Opt. Express **16**, 5757 (2008).